

Non-homogeneous pairing in disordered two-band s-wave superconductors

Heron Caldas¹, S. Rufo², and M. A. R. Griffith²

*Departamento de Ciências Naturais,
Universidade Federal de São João Del Rei,
Praça Dom Helvécio 74, 36301-160,
São João Del Rei, MG, Brazil*

and

*Centro Brasileiro de Pesquisas Físicas,
Rua Dr. Xavier Sigaud, 150 - Urca,
22290-180, Rio de Janeiro, RJ, Brazil*

(Dated: March 6, 2024)

We investigate the effects of disorder in a simple model of a hybridized two-dimensional two-band s-wave superconductor. We take into account the situations in which these bands are formed by electronic orbitals with angular momentum such that the hybridization $V(\mathbf{k})$ among them is anti-symmetric, under inversion symmetry. The impurity potential is given by an independent random variable W which controls the strength of the on-site disorder. We find that while the random disorder acts in detriment of superconductivity, hybridization proceeds favoring superconductivity. This shows that hybridization, which may be induced by pressure or doping, plays an important role in two-band models of superconductivity, making them eligible candidates to describe real materials. We also find that in moderate and strong disorder, the system is broken into islands, with correlated local order parameters. These correlations persist to distances of several order lattice spacing which corresponds to the size of the SC-islands.

I. INTRODUCTION

The experimental discovery of high transition temperature in superconducting oxides [1] and the subsequent discoveries of strontium ruthenate [2], magnesium diboride [3], and iron pnictides [4, 5] has motivated an intense theoretical investigation in the superconducting properties of these materials. Experiments have indicated that one of these compounds, magnesium diboride (MgB_2), with a transition temperature of ≈ 40 K [6], has two distinct superconducting gaps [7–13] and, consequently, was classified as a two-band superconductor (SC) [14].

Since in MgB_2 the relevant coupling mechanism is of intra-band character [15], two-band models have been employed to investigate materials possessing two pairing gaps. As pointed out in Ref. [16], the number of different gaps that emerge in multi-orbital systems is a direct consequence of the hybridization among the orbitals present in a given material. In fact, as shown in Ref. [17], the Fermi surface (FS) of MgB_2 is determined by three orbitals, nevertheless only two different BCS gaps are experimentally observed. This happens because two of the three orbitals hybridize with each other forming one single band, responsible for a large superconducting gap on the σ FS, while the non-hybridized orbital is related to the smaller superconducting gap at the π band FS.

It is worth to mention that besides intermetallic binary superconductors such as MgB_2 , angle-resolved photoelectron spectroscopy (ARPES) experiments on La-based cuprates (with the hybridization of $d_{x^2-y^2}$ and d_{z^2} orbitals) provided direct observation of a two-band structure in these compounds [18].

It is well known that disorder has tremendous conse-

quences on conductors and superconductors. In a metal, the effect of disorder is to induce the Anderson localization of the electrons transforming a metal into an insulator, while in superconductors pair-localization results in superconductor-insulator transition (SIT). In very strong disorder the Cooper pairs can get localized due to the fractal nature of the single-particle near-critical wave function [19–21]. Thus, the effects of disorder in a superconductor brings about a competition of long-range phase coherence between electron pair states of the superconducting phase and the limitation of the spatial extent of the wave functions due to localization [22]. Then, it is natural to expect a critical disorder at which superconductivity is overcome. It was shown by Anderson [23] and Abrikosov and Gorkov (AG) [24] that nonmagnetic impurities have no significant effect on the superconducting transition temperature. However, Anderson's and AG theory are applicable only to weakly disordered systems [25]. The problem of a (one-band) s-wave superconductor in the presence of a random potential has been investigated for weak and strong disorder in Ref. [26]. They found that in the high-disorder regime, the system breaks up into superconducting islands, separated by an insulating sea.

In this paper we investigate the effects of disorder in the superconducting properties of a simple two-band model, subjected to the hybridization of two single bands, namely a and b . We consider superconducting (s-wave) interactions only inside each band, which will result in intra-band pairing gaps Δ_a and Δ_b , respectively, in these bands. The immediate consequence of hybridization is to transfer the quasiparticles among the bands and the clear advantage is that it can be adjusted experimentally by external factors like pressure or doping [27]. Indeed, experiments in cuprates have shown that its transition tem-

perature is very sensitive to an applied (external) pressure, which is responsible for the hybridization between the d orbitals of the cooper and the p orbitals of the oxygen [28, 29]. We appraise antisymmetric, k -dependent hybridization $V(k)$, that in the position space is translated to $V_{ij} = -V_{ji}$. This choice is due to the fact that the antisymmetric hybridization produces an odd-parity mixing between the a and b bands, and is responsible for the p -wave nature of an induced inter-band gap [30]. 1D models with a pairing gap possessing p -wave symmetry are highly desired for the investigation of the appearance of Majorana zero-energy bound states [31–34].

Using the Bogoliubov-de Gennes (BDG) mean-field theory we show the distribution of the local pairing amplitude $P(\Delta)$ and density of states $N(\omega)$ for various hybridization and disorder strengths. We analyze how a (random) disorder modifies the behavior of the superconducting two-band model. We have found that while the random disorder is detrimental to superconductivity, hybridization favors superconductivity. We also found that in the case of high disorder, the system breaks into correlated islands in a insulating sea. This fact is known already for a one-band system. The novelty here is that there is correlations between the a and b pairing regions, due to hybridization, and even the correlations between a and a pairing islands (and the same for b and b) calculated here depend on the hybridization.

The rest of this paper is organized as follows: In Sec. II we describe our two-band model for the disordered SC and describe the inhomogeneous BdG mean-field method. In this section we also obtain the BdG equations. Our results are shown in Sec. III. We conclude in Sec. IV.

II. MODEL HAMILTONIAN

We describe a generic two-band SC in two-dimensions ($2D$) by a Hubbard-type Hamiltonian, which is given by

$$\begin{aligned}
 H = & - \sum_{\langle i,j \rangle, \sigma} t_{ij}^a a_{i\sigma}^\dagger a_{j\sigma} - \mu_a \sum_{i,\sigma} a_{i,\sigma}^\dagger a_{i,\sigma} \\
 & - \sum_{\langle i,j \rangle, \sigma} t_{ij}^b b_{i,\sigma}^\dagger b_{j,\sigma} - \mu_b \sum_{i,\sigma} b_{i,\sigma}^\dagger b_{i,\sigma} \\
 & + \sum_{\langle i,j \rangle, \sigma} V_{ij} (b_{i,\sigma}^\dagger a_{j,\sigma} + a_{i,\sigma}^\dagger b_{j,\sigma}) \\
 & - U_a \sum_i n_{i,\uparrow}^a n_{i,\downarrow}^a - U_b \sum_i n_{i,\uparrow}^b n_{i,\downarrow}^b, \quad (1)
 \end{aligned}$$

where $a_{i\sigma}^\dagger (a_{j\sigma})$ and $b_{i\sigma}^\dagger (b_{j\sigma})$ are the fermionic creation (annihilation) operator at site \mathbf{r}_i for the a and b bands, respectively. The lattice parameter for the square lattice is $a = 1$, and spin $\sigma = \uparrow\downarrow$. $\mu_a = \mu + E_a$ and $\mu_b = \mu + E_b$ are the chemical potentials, where E_a and E_b are the bottom of the a and b bands. $n_{i,\sigma}^a = a_{i\sigma}^\dagger a_{i\sigma}$ and $n_{i,\sigma}^b = b_{i\sigma}^\dagger b_{i\sigma}$

are the density operators, t_{ij}^a and t_{ij}^b are the hopping integrals between sites i and nearest neighbor j for the a and b electrons. $U_a (U_b)$ is the onsite attractive potential between the $a(b)$ electrons. V_{ij} is the (k -dependent) nearest neighbours hybridization of the two bands, which may be symmetric or antisymmetric, arising from a non-local character of the mixing. Notice that in Hamiltonian in Eq. (1) we have neglected the (rather involved) effects of Coulomb repulsion [26]. However, as will be clear below, even with such a simplification, the hybridized two-band model with attractive intra-band interactions and with disorder shows very interesting results which were worth to be investigated.

A. The Mean Field Theory

The interaction part of the Hamiltonian in Eq. (1) possesses products of four fermionic operators, which can be decoupled by the Hartree-Fock (HF) BCS decoupling (see appendix A) of two-body terms [35, 36]. The decoupling procedure generates the mean field Hamiltonian (MFH) H_{MF} below

$$\begin{aligned}
 H_{MF} = & - \sum_{\langle i,j \rangle, \sigma} t_{ij}^a a_{i\sigma}^\dagger a_{j\sigma} - \sum_{i,\sigma} (\tilde{\mu}_a - W_i) a_{i\sigma}^\dagger a_{i\sigma} \\
 & - \sum_{\langle i,j \rangle, \sigma} t_{ij}^b b_{i,\sigma}^\dagger b_{j,\sigma} - \sum_{i,\sigma} (\tilde{\mu}_b - W_i) b_{i,\sigma}^\dagger b_{i,\sigma} \\
 & - \sum_{\langle i,j \rangle, \sigma} V_{ij} (b_{i,\sigma}^\dagger a_{j,\sigma} + a_{i,\sigma}^\dagger b_{j,\sigma}) \\
 & + \sum_i [\Delta_{a,i} a_{i,\uparrow}^\dagger a_{i,\downarrow}^\dagger + \Delta_{a,i}^* a_{i,\downarrow} a_{i,\uparrow}] \\
 & + \sum_i [\Delta_{b,i} b_{i,\uparrow}^\dagger b_{i,\downarrow}^\dagger + \Delta_{b,i}^* b_{i,\downarrow} b_{i,\uparrow}], \quad (2)
 \end{aligned}$$

where we have included the same local impurity potential W_i in both a and b bands, and $\tilde{\mu}_p = \mu_p + U_p < n_i^p > /2$, where $p \equiv a, b$. Here $< n_i^p >$ is the average of the occupation number. The impurity potential is defined by an independent random variable W_i uniformly distributed over $[-W, W]$, at each site r_i . W thus controls the strength of the disorder. In this way, one can think of effective *local* chemical potentials given by $\mu_{p,i}^{eff} \equiv \tilde{\mu}_p - W_i$ that, as we will see below, are responsible, together with the intra-band interaction U_p and hybridization V_{ij} , for the rich physics and interesting phase diagrams we find. For simplicity, but without loss of generality, we assume that $t_{ij}^a = t_{ij}^b = t$. Besides, the strength of the hybridization is given by V . Then, the MFH in Eq. 2 describes a hybridized two-band s-wave superconductor, under the influence of random *nonmagnetic* impurities, by means of an attractive Hubbard model, pictorially described in Figure 1.

In order to diagonalize H_{MF} in Eq. (2) for n^2 (n sites along x direction and n sites along y

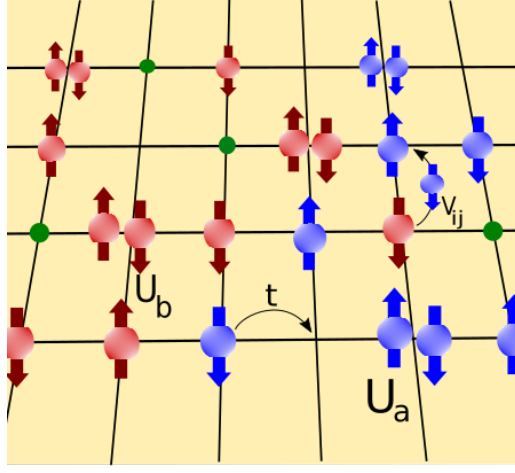


FIG. 1. (Color online) Schematic representation of the hybridized two-band attractive Hubbard model in the presence of disorder. Electrons from a (blue) and b (red)-bands can hop between lattice sites (having lattice spacing a) with a hopping parameter t . The hybridization V_{ij} destroys an electron of band $a(b)$ and creates one in band $b(a)$ (without spin-flip), in a nearest neighbor site. Due to Pauli's principle, both hopping and hybridization are only possible if the final lattice site is empty or occupied with an electron with a different spin. The green marbles represent nonmagnetic impurities randomly distributed on the square lattice. Two electrons of band- $a(b)$ with opposite spin localized at the same lattice site have an intra-band on-site interaction strength $U_{a(b)}$. As an example, it is shown in the figure that with the action of V_{ij} a spin-down electron from band- b has been annihilated and created in band- a in a nearest neighbor site, that has already a spin-up electron from band- a . This “blue pair” will now experience the interaction potential U_a .

direction) sites, we firstly express Eq. 2 in matrix form $H_{MF} = \Psi^\dagger \mathcal{H} \Psi$, such that $\Psi^T = (a_{1\uparrow}^\dagger, \dots, a_{n2\uparrow}^\dagger, b_{1\uparrow}^\dagger, \dots, b_{n2\uparrow}^\dagger, a_{1\downarrow}, \dots, a_{n2\downarrow}, b_{1\downarrow}, \dots, b_{n2\downarrow})$. The MFH can be diagonalized by the transformation $M^\dagger \mathcal{H} M = \text{diag}(-E_1 \dots -E_{2N}; E_{2N+1} \dots E_1)$ for $N = n^2$, see appendix B.

The matrix elements of M can be related to coefficients of the Bogoliubov-Valatin transformation [37]. Using the Bogoliubov-Valatin transformation defined in appendix B, the local particle densities and local pairing gaps can be expressed as

$$\langle n_i^a \rangle = 2 \sum_{n'=1}^N [|M_{i,2N+n'}|^2 f + |M_{i,3N+n'}|^2 (1-f)] \quad (3)$$

$$\langle n_i^b \rangle = 2 \sum_{n'=1}^N [|M_{i+N,2N+n'}|^2 f + |M_{i+N,3N+n'}|^2 (1-f)] \quad (4)$$

$$\Delta_{a,i} = U_a \sum_{n'=1}^N [M_{i,2N+n'} M_{i+2N,2N+n'} (1-2f)] \quad (5)$$

$$\Delta_{b,i} = U_b \sum_{n'=1}^N [M_{i+N,2N+n'} M_{i+3N,2N+n'} (1-2f)], \quad (6)$$

where $f \equiv f(E_{n'}) = 1/(e^{\beta E_{n'}} + 1)$, with $\beta = 1/k_B T$, is the Fermi function. The equations above form a system of $4N$ self-consistent equations. We numerically solved

theses equations for a lattice with $N = 144$ and $N = 400$ sites. The size of the matrix \mathcal{H} is $4N \times 4N$ and, therefore, needed a huge computational effort.

In the numerical simulations we have used an antisymmetric hybridization such that $V_{ij} = -V_{ji}$. This choice is appropriate for our model to describe, for example, the s and p -orbitals, which hybridizes in different sublattices [38, 39].

III. RESULTS

A. Clean systems

The solutions of Eqs. (3), (4), (5) and (6) provide N values for Δ_a , Δ_b , n_a and n_b . We defined a Distribution of the Local Pairing Amplitude (DOLPA), which tell us how homogeneous will be the order parameters Δ_p in the whole lattice.

In Fig. 2 (a) and (b) we show DOLPA for Δ_a (blue) and Δ_b (red) for a clean system $W/t = 0$. Note that, when the disorder and hybridization are zero, see Fig. 2 (a), all (Δ_a, Δ_b) possesses values equal to $(0.309, 0.361)$, and therefore, the system will present a homogeneous superconducting phase.

Keeping $W/t = 0$, when we turn on the hybridization to $V/t = 2.0$, see Fig. 2 (b), both the superconducting order parameters Δ_a and Δ_b are reduced. On the other hand, it is worth to comment that for a different set of parameters our numerical analysis shows that the hybridization is also able to increase the order parameters

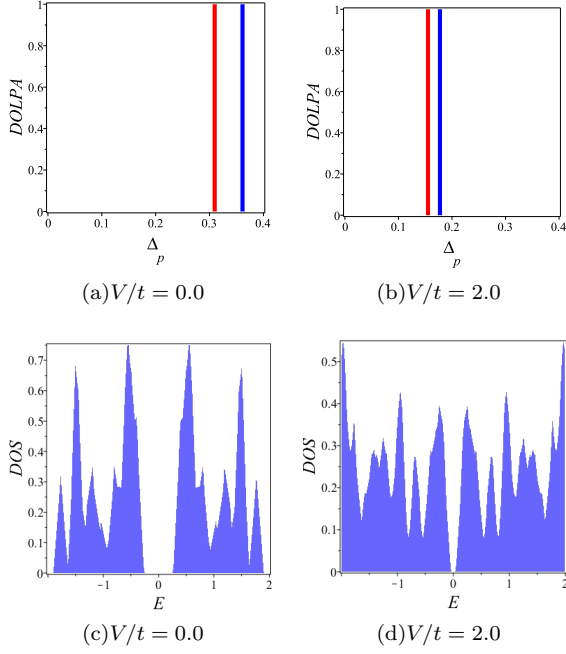


FIG. 2. (Color online) Distribution of the local pairing amplitude DOLPA for a clean system $W/t = 0$ and for $V/t = 0.0$ and $V/t = 2.0$. We set $N = 144$, $U_a/t = 3.5$ and $U_b/t = 3$. Blue curve is DOLPA for $p = a$, while the red curve for $p = b$. (a) Local pairing amplitude for $V/t = 0.0$, (b) Local pairing amplitude for $V/t = 2.0$, (c) Density of states for $V/t = 0.0$ and (d) Density of states for $V/t = 2.0$.

Δ_p (for instance $U_a/t = 3$, $U_b/t = 4$ and $V/t = 0.5$). This reflects a non-monotonic behavior of the order parameters with respect to hybridization. Therefore, there are two regimes that depend on the magnitude of the hybridization. Indeed, there exists a V^* such that the pairing gaps $\Delta_a(V^*)$ and $\Delta_b(V^*)$ are maximum [30, 40]. In the next section, we will discuss that in both regimes the hybridization term makes the systems robust against the disorder potential, regarding the case with zero hybridization. The superconducting phase is sensitive to local perturbations in both orbitals. Since the hybridization acts connecting electrons from orbitals a and b , the correlations $\langle a_{\sigma,i}^\dagger b_{\sigma,i} \rangle$ and $\langle a_{\uparrow,i} a_{\downarrow,i} \rangle$ and $\langle b_{\uparrow,i} b_{\downarrow,i} \rangle$ becomes strongly depending on the hybridization. Again, the DOLPA shows a homogeneity characteristic of systems without local perturbations or disorder effects, see Fig. 2 (b).

Finally, we show the local density of states (DOS) in Fig. 2 (c) $V/t = 0$ and (d) $V/t = 2.0$. There is a gap region around the $E = 0$ in the DOS. Note that the gap region decreases when the hybridization increases (i.e. $\Delta_E = 0.2$ for $V/t = 0$ while Δ_E almost vanishes for $V/t = 2.0$).

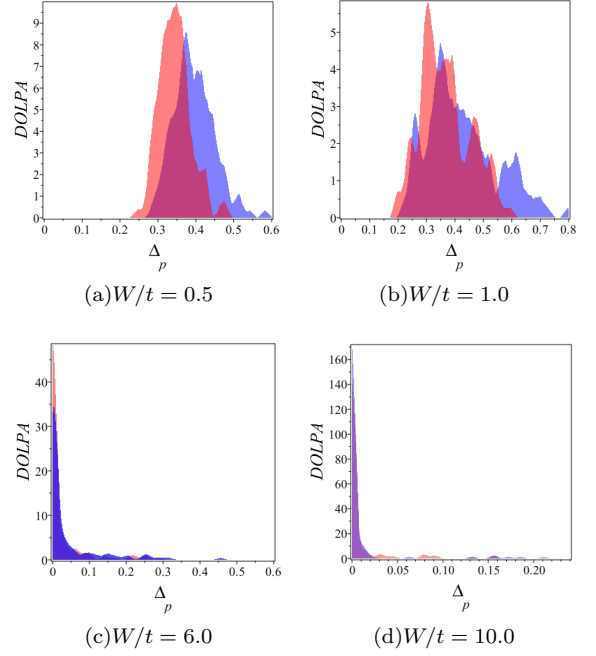


FIG. 3. (Color online) Distribution of the local pairing amplitudes DOLPA for various disorder strengths W/t and for $V/t = 0$. We set $N = 144$, $U_a/t = 3.5$ and $U_b/t = 3$. The blue curve is DOLPA for $p = a$, while the red curve is for $p = b$. (a) $W/t = 0.5$, (b) $W/t = 1.0$, (c) $W/t = 6.0$ and (d) $W/t = 10.0$.

B. Disordered systems

We now investigate the systems in which both a and b -bands have the same *effective* chemical potential and, consequently, are affected by the same sort of (random) disorder in each site, that is $\tilde{\mu}_a = \tilde{\mu}_b = \mu - W_i$.

In Fig. 3 we show the distribution of the local pairing amplitudes for various disorder strengths $W/t = 0.5, 1.0, 6.0$ and 10 , and for hybridization $V/t = 0$. The blue curve is the distribution of the local pairing amplitude Δ_a , while the red curve is the distribution of the local pairing amplitude for Δ_b . Notice that as the disorder strength increases, from (a) to (d), the pairing amplitudes begin to concentrate around $\Delta_p = 0$, showing that strong disorder is deleterious for the superconducting state also in a two-band decoupled model.

In Fig. 4 we show the density of states for the dirty system without hybridization and several disorder strength $W/t = 0.5, 1.0, 6.0$ and 10 , as in Fig. 3, since these figures share the same set of parameters. Accordingly, we can observe the presence of an energy gap for each case.

In order to verify the effect of hybridization on the distribution of the local pairing amplitudes and the density of states, we present these results in Fig. 5 and Fig. 6.

Fig. 5 shows the distribution of the local pairing amplitudes DOLPAR for various disorder strengths W and for hybridization $V/t = 2.0$. The blue curve is the distri-

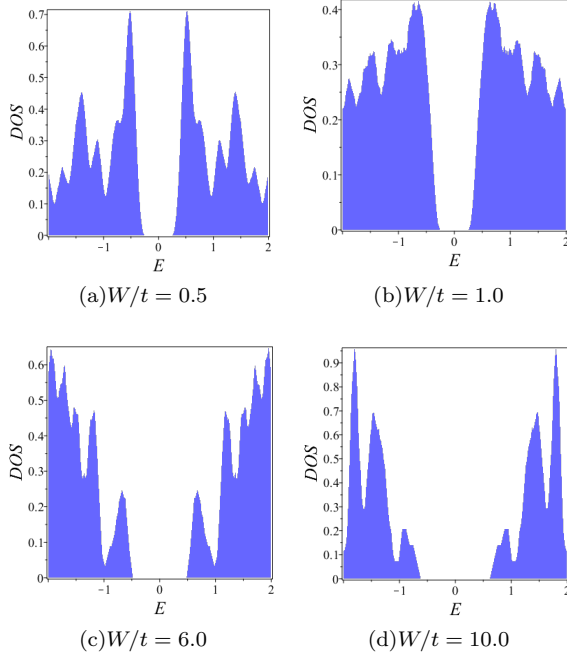


FIG. 4. (Color online) Density of states $N(\omega)$ for four disorder strengths W/t and hybridization $V/t = 0$. Here, we have $N = 144$ sites, $U_a/t = 3.5$ and $U_b/t = 3$. Note that the spectral energy gap remains finite even at large W/t . (a) $W/t = 0.5$, (b) $W/t = 1.0$, (c) $W/t = 6.0$ and (d) $W/t = 10.0$.

bution of the local pairing amplitude Δ_a , while the red curve is the distribution of the local pairing amplitude Δ_b . Notice that for low values of disorder, (a) $W/t = 0.5$ and (b) $W/t = 1.0$, the pairing amplitudes begin to spread around the same value, approximately $\Delta_p = 0.15$. Interestingly, as the disorder keeps increasing, (c) $W/t = 6.0$ and (d) $W/t = 10.0$, both Δ_a and Δ_b remain nonzero, showing that the hybridization acts favoring superconductivity against disorder (see in Fig. 3 c) and d) that when $V/t = 0$, the majority of Δ_p is around zero amplitude). This could be expected, since antisymmetric hybridization may increase the pairing gaps of a two band model (without disorder) for a certain range of the hybridization strength [30, 40]. We verified that even in the range of the strength of the hybridization that decreases the pairing gaps the system is robust against disorder, when compared to same values of disorder in non-hybridized systems, i.e., in two single (decoupled) a and b bands. In addition, the results shown in Fig. 6 still present finite energy gap at large values of W/t .

After a numerical inspection in Fig. 4 and Fig. 6, one can verify that the hybridization V/t , disorder W/t , and the gap energy ΔE possess a complex relationship. In particular, if $W/t = 0.5$, the energy gap is given by $\Delta_E = 0.298$ for $V/t = 0.0$, while it is greatly diminished for $V/t = 2.0$ ($\Delta_E = 0.16$). By comparing these energy gap values, given the respective values of V/t and for a fixed W/t , we can deduce that the hybridization, at least

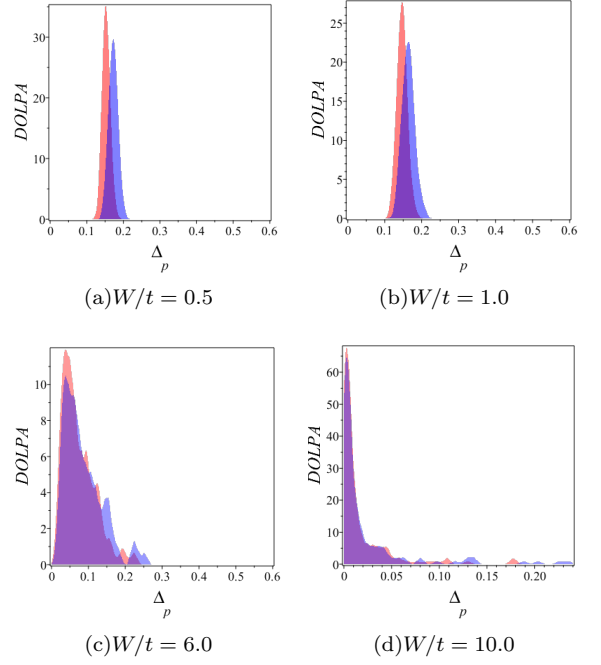


FIG. 5. (Color online) Distribution of the local pairing amplitude for various disorder strengths W/t and for hybridization $V/t = 2.0$. Here, we have $N = 144$ sites, $U_a/t = 3.5$ and $U_b/t = 3$. Blue curve is distribution of the local pairing amplitude for $p = a$, while the red curve is distribution of the local pairing amplitude for $p = b$. (a) $W/t = 0.5$, (b) $W/t = 1.0$, (c) $W/t = 6.0$ and (d) $W/t = 10.0$.

in the analyzed values, tends to result in an energy gap decreasing.

In Fig. 7 (a) and (b) we show the phase diagram in the $(W/t, V/t)$ plane, while (c) and (d) in the $(W/t, U_a/t)$, for fixed $\mu/t = 0.1$ and $U_b/t = 3.0$. The contour plot indicates the percentage of sites with local pairing amplitude $\Delta_a = 0$ and $\Delta_b = 0$. The percentage bar varies from 0% (white) for the pure superconducting state (SC) to 100% (black) for a fully insulating state (I), while intermediate percentage values correspond to a kind of intermediate state (yellow and red). Note that in the phase diagrams in Fig. 7 (c) and (d), obtained from our two-band model, the behaviors are consistent with the one obtained for one band in Ref. [26] (see Figure 15 inside this reference, where disorder is designated by V/t which is the same as W/t in the present work). In both cases, we observed the presence of a s-wave superconducting and gapped insulating phases. In special, by comparing our phase diagrams in Fig. 7 (c) and (d) with the one in Ref. [26] (Fig. 15) one can identify additional regions that can support SC-Islands (intermediate phase in yellow and red) beyond the pure superconducting and insulating phases (SC and I in white and black, respectively). Besides, our phase diagrams in Fig. 7 (c) and (d) demonstrate the possibility of the occurrence of a kind of reentrant superconductor-insulator transition [41] with decreasing U_a/t [42].

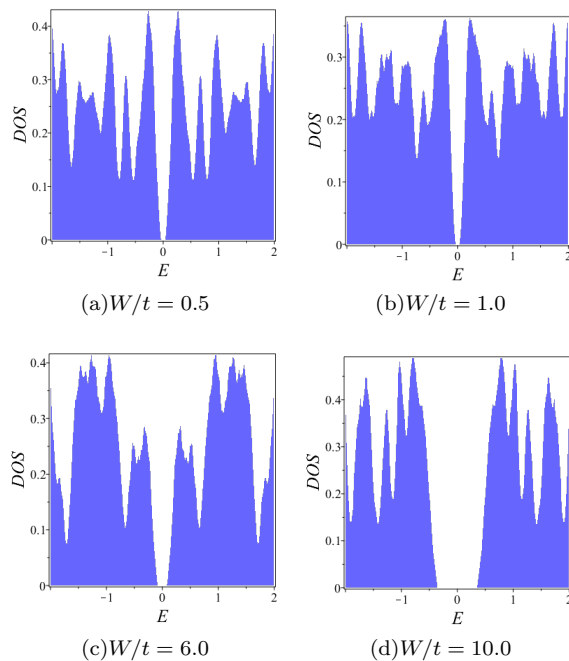


FIG. 6. (Color online) Density of states $N(\omega)$ for four disorder strengths W/t and hybridization $V/t = 2.0$. Here, we have $N = 144$ sites, $U_a/t = 3.5$, $U_b/t = 3$. Surprisingly, the increase of hybridization enhances the local superconducting order parameters making the whole system more robust against the disorder and the energy gap remains finite even at large W/t . (a) $W/t = 0.5$, (b) $W/t = 1.0$, (c) $W/t = 6.0$ and (d) $W/t = 10.0$.

Notice that in Figures 7 (a) and (b), there is a pure superconducting state for $W/t < 1.5$ for all values of V/t analyzed, and for $W/t < 1.0$ in (c) and (d), for all values of U_a/t , showing the regions of applicability of Anderson's theorem.

To have a better understanding of the competition between the effects of disorder and hybridization in the whole system, we present in Fig. 8 a heatmap plot of the local densities n_a and n_b ; local pairing amplitude Δ_a and Δ_b as a function of hybridization, for a fixed $W/t = 6.0$, $\mu/t = 0.1$ and an ensemble of nine disorder realizations of 20×20 lattices. (a) Local densities and (b) Local pairing amplitudes for hybridization $V/t = 0.1$, where we highlight the regions I-Insulating ($\Delta_a = 0$ and $\Delta_b = 0$), II-mixed-superconducting ($\Delta_a \neq 0$ and $\Delta_b \neq 0$), III-superconducting type b ($\Delta_a = 0$ and $\Delta_b \neq 0$), IV and V-superconducting type a ($\Delta_a \neq 0$ and $\Delta_b = 0$). (c) Local densities and (d) Local pairing amplitudes for hybridization $V/t = 0.5$. We then identify the presence of (local) superconducting islands (SC-Islands) in regions II, IV, and V, separated by an insulating region. We observed that the presence of the SC-Islands is favored by the increasing of U_a/t and W/t and correspond to the intermediate phase in Fig. 7 (yellow and red regions).

It is important to note, by comparing Fig. 8(b) and (d), that the increasing of the hybridization favors the II-

mixed-superconducting region. For this reason the spatial fluctuation of the lattice is modified. These complex structures of formation of superconducting and mixed islands and an insulating "medium" reveals a highly non-homogenous formation.

Accordingly, as the disorder potential W/t is randomly assigned for each site we have uncorrelated local densities n_a and n_b , as we can see in Fig. 8 (a) and (c) with the absence of cluster formation [26]. Despite that, due the self-consistent approach the local pairing amplitudes Δ_a and Δ_b present a spatial correlation between the SC-islands (regions II, III, IV and V in Fig. 8 (b)). This correlation occurs from moderate to high disorder values, in this case $W/t = 6.0$. The typical size of a SC-Island is of the order of the coherence length ξ which is subject to the disorder potential W/t as well as the effective electron attraction U_a/t and U_b/t .

Thus, from Fig. 8 (b) and (d) we can see how the appearance of disorder implies in a strong spatial fluctuation of the local order parameters Δ_p . In Fig. 9 (a) and (b) we show the spatial fluctuations for $V/t = 0.1$ and $V/t = 0.5$, respectively. The strong spatial fluctuation structure reveals where the order parameter get a large amplitude, blue for Δ_a , red for Δ_b and assuming a purple color where the SC-Island are in superposition. These SC-Island are correlated and we present the results showing this fact in Fig. 9, as the disorder-averaged correlation functions $\overline{\Delta_{a,i}\Delta_{a,j}}$ (c), $\overline{\Delta_{b,i}\Delta_{b,j}}$ (d) and $\overline{\Delta_{a,i}\Delta_{b,j}}$ (e). The average is performed for each set of $\Delta_{p,i}\Delta_{p',j}$ that share the same spatial distance $|r_i - r_j|$. The thin curves correspond to the correlation function for $V/t = 0.1$ of spatial fluctuations in Fig. 9 (a) and the thick curves for $V/t = 0.5$ of spatial fluctuations in Fig. 9 (b). Note that as the hybridization is increased from $V/t = 0.1$ to $V/t = 0.5$ the correlations curves $\overline{\Delta_{a,i}\Delta_{a,j}}$, $\overline{\Delta_{b,i}\Delta_{b,j}}$ and $\overline{\Delta_{a,i}\Delta_{b,j}}$ are closer. Besides, the coherent tunneling of the Cooper pairs between the SC-Islands is responsible for the establishment of correlation [43]. On the other hand, the regions with a relative small Δ_p behave as an insulating phase with unpaired Cooper pair electrons. It is important to remark that we did not take into account quantum fluctuations in the phase ϕ of the order parameter (that would imply in gap parameters given by $\tilde{\Delta}_p = e^{i\phi}\Delta_p$), which are expected to destroy the long-range phase coherence between the small SC islands for very large disorder [26, 43].

C. Experimental Consequences

It is also important to discuss the experimental aspects of our two-band model subjected to disorder and hybridization. It is experimentally doable to grow homogeneously disordered films [44] that are disordered both on an atomic scale and granular films [45, 46]. These two types of films will essentially depend on the material, the substrate, and growth conditions [26] as, for example, a film of 99.99% Sn (or Pb) evaporated onto fire-

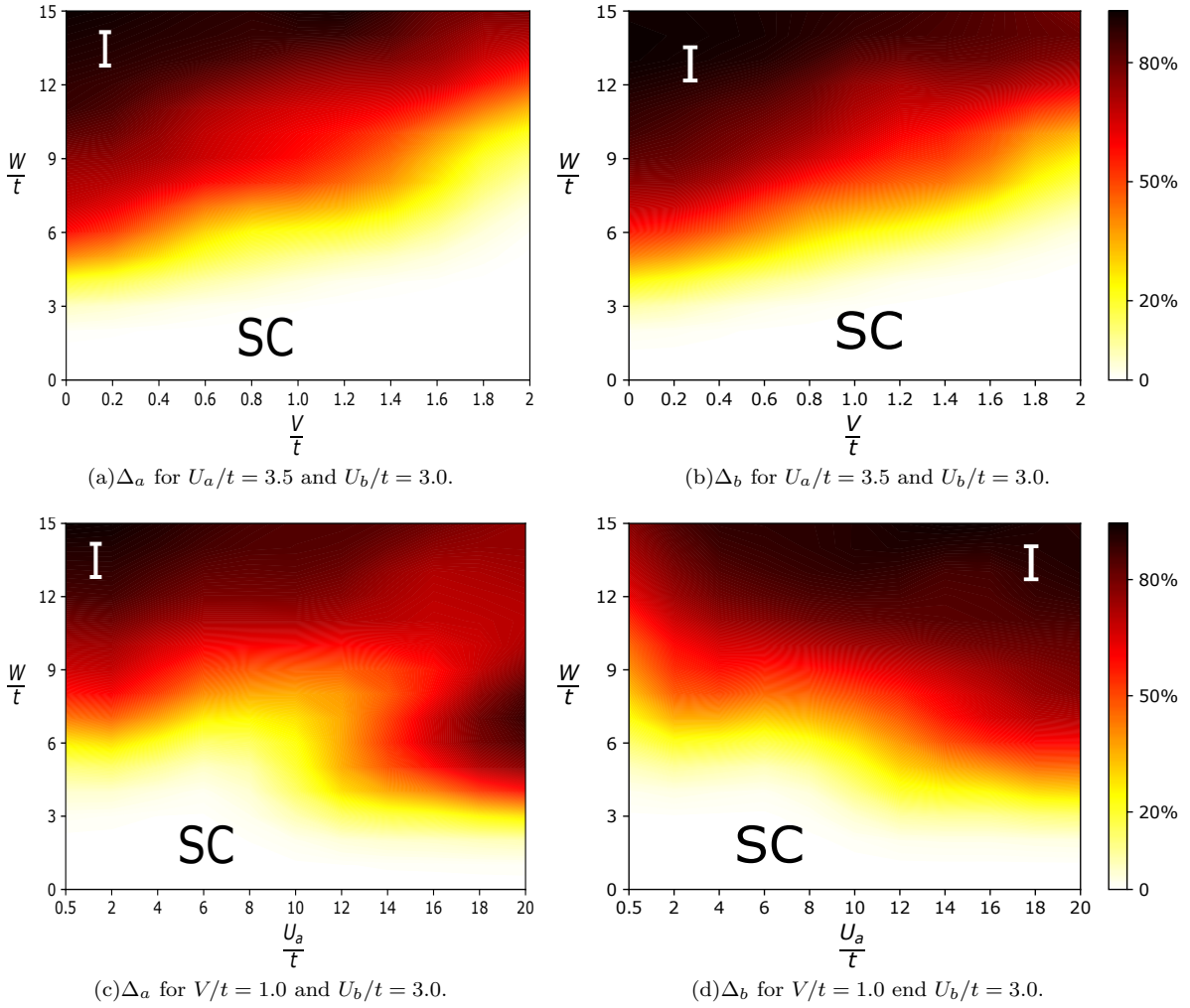


FIG. 7. (Color online) Phase diagram for the hybridized two-band model of superconductivity in the presence of disorder W/t for a fixed $\mu/t = 0.1$, $U_b/t = 3.0$ and for an ensemble of nine realizations of 20×20 lattices. The contour plot represents the percentage of sites with local pairing amplitude $\Delta_a = 0$ and $\Delta_b = 0$.

polished glass substrates [45], or a 99.997% amorphous indium-oxide (In_2O_3) samples evaporated onto a SiO_2 substrate [47]. In these experiments [44, 46], the effective disorder was controlled by changing the film thickness.

In the present case, the phase diagram of Fig. 7 could be useful as a guide to experimental measurements in order to identify regions with SC-Islands features. A possible experimental goal is the realization of the superconducting phase only of the type a with Δ_a , described by the correlation $\langle a_{\uparrow,i} a_{\downarrow,i} \rangle$ (or only of the type b with Δ_b , described by the correlation $\langle b_{\uparrow,i} b_{\downarrow,i} \rangle$) and then, the mixed-superconducting phase. In contrast with the one-band model studied in Ref. [26], we remark that the mixed-superconducting phase appeared only in the context of the highly hybridized two-band model, as explored here. We expect that landscapes showing the regions with insulating, superconducting, and mixed-superconducting islands should be visible through scanning tunneling microscopy (STM), as the topography im-

ages of a ‘ π' ’-shaped Pb island sitting on top of a striped incommensurate (SIC) surface [48].

IV. CONCLUSION

In this paper we investigated the effects of disorder in the superconducting properties of a simple hybridized two-band model. We considered the situations in which these bands are formed by electronic orbitals with angular momentum such that the hybridization $V(\mathbf{k})$ among them is antisymmetric under inversion symmetry. We studied the effect of both disorder and an antisymmetric hybridization in the cases where there is s-wave intra-band interactions only inside each of the two bands. The impurity potential is given by an independent random variable W which controls the strength of the disorder. In some recent experiments, the effective disorder was controlled by varying the film thickness. On the other hand,

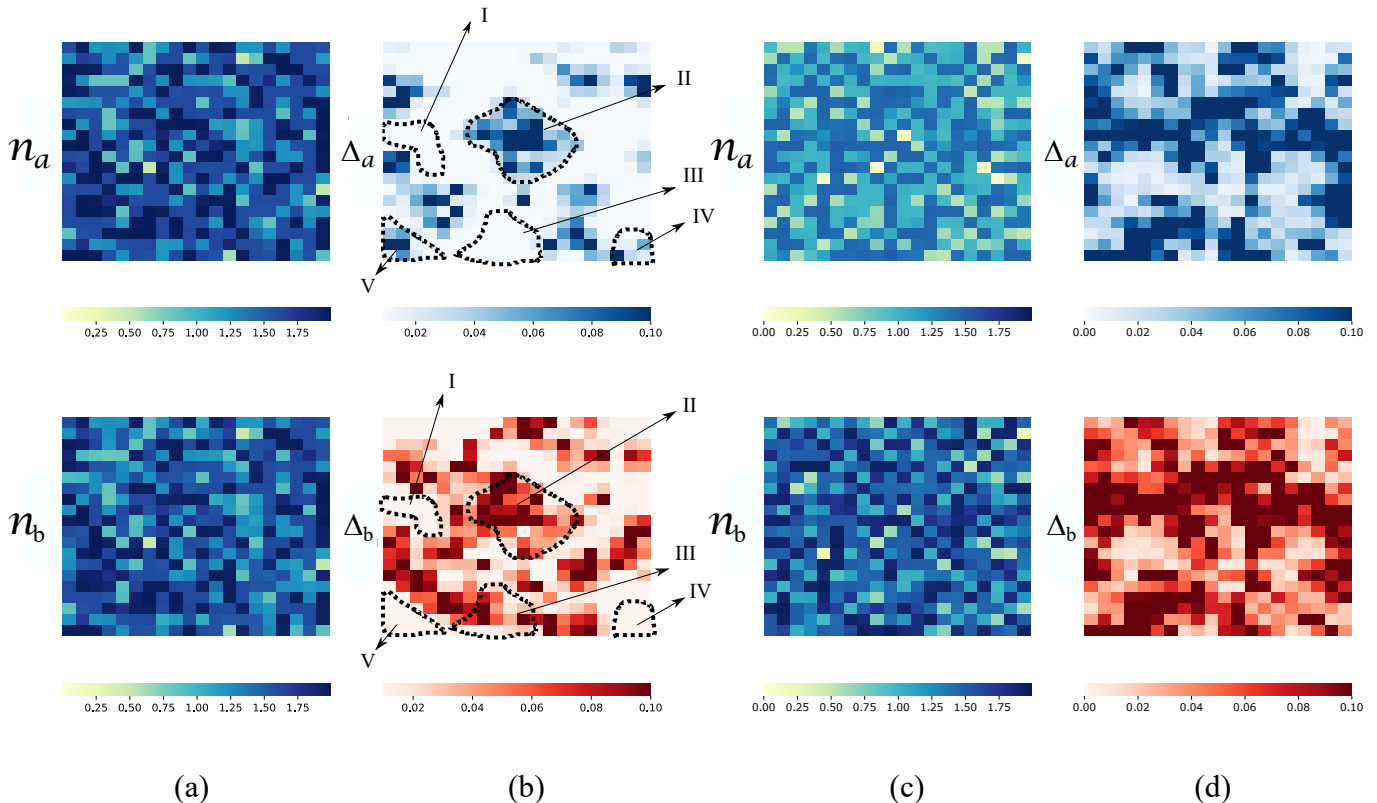


FIG. 8. (Color online) Local densities n_a and n_b ; local pairing amplitudes Δ_a and Δ_b as a function of hybridization, for a fixed $W/t = 6.0$, $\mu/t = 0.1$ and an ensemble of nine disorder realizations of 20×20 lattices. (a) Local densities and (b) Local pairing amplitudes for hybridization $V/t = 0.1$, where we highlight the regions I-Insulating ($\Delta_a = 0$ and $\Delta_b = 0$), II-mixed-superconducting ($\Delta_a \neq 0$ and $\Delta_b \neq 0$), III-superconducting type b ($\Delta_a = 0$ and $\Delta_b \neq 0$), IV and V-superconducting type a ($\Delta_a \neq 0$ and $\Delta_b = 0$). (c) Local densities and (d) Local pairing amplitudes for hybridization $V/t = 0.5$. The regions II, IV and V denote the superconducting islands (SC-Islands). The SC-Islands corresponds to the intermediate phase in Fig. 7 (yellow and red regions). Note that the increase of the hybridization favors the II-mixed-superconducting region.

the hybridization between the two-bands can be tunable by applying strain or by carrier doping. We found that while (the random disorder) W acts in detriment of superconductivity (driving to zero the pairing gap parameter through a suppression of the superconducting phase in favor of an insulating one), hybridization makes the system more robust against disorder effects.

We also found that strong disorder implies in a prominent spatial fluctuation of the local order parameters Δ_a and Δ_b , which are correlated. These correlations perseverate to distances of several order lattice spacing which corresponds to the size of the SC-Islands.

An interesting theoretical extension of this work could be to consider this two-dimensional two-band hybridized system in the presence of disorder under a static magnetic field h parallel to the 2D plane [49]. Given the variety of external effects, hybridization V , disorder W and magnetic field h , we hope that new and possibly exotic phases will appear. An investigation in this direction

is intriguing and will be the subject of future work.

V. ACKNOWLEDGMENTS

We thank D. Nozadze and N. Trivedi for enlightening discussions. We wish to thank CAPES and CNPq, Brazil, for partial financial support.

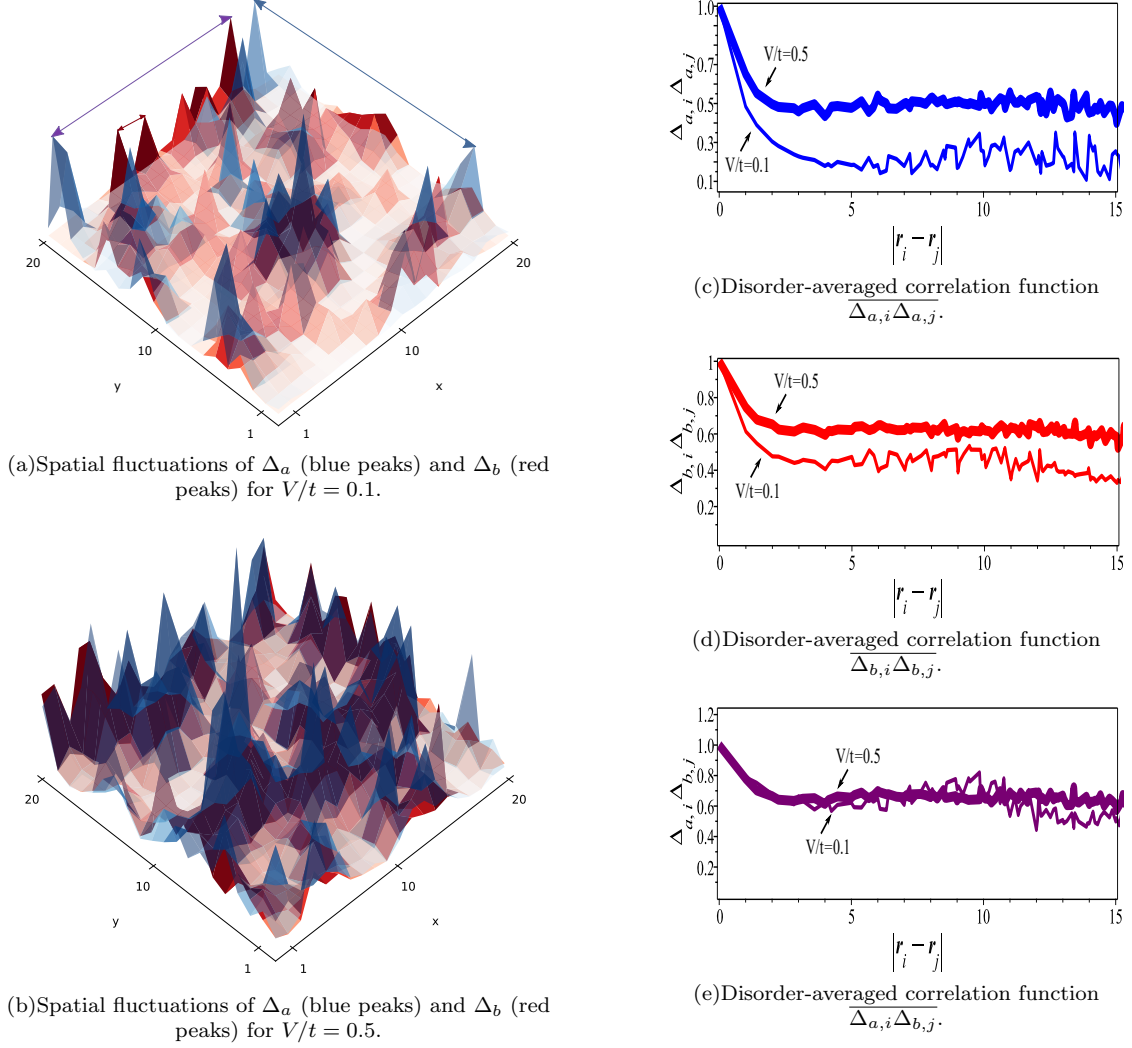


FIG. 9. (Color online). Spatial fluctuations of the local pairing amplitudes Δ_a and Δ_b in a 20×20 lattice, for $V/t = 0.1$ (a) and $V/t = 0.5$ (b). Following Fig. 8, we set $W/t = 6.0$ and $\mu/t = 0.1$. The blue arrows denote the coherent tunneling between $\Delta_{a,i}$ and $\Delta_{a,j}$ (blue peaks), the red arrows denote the coherent tunneling between $\Delta_{b,i}$ and $\Delta_{b,j}$ (red peaks) as well as the purple arrows denote the coherent tunneling between $\Delta_{a,i}$ and $\Delta_{b,j}$ (blue and red peaks). We present the disorder-averaged correlation function $\overline{\Delta_{a,i} \Delta_{a,j}}$ (c), $\overline{\Delta_{b,i} \Delta_{b,j}}$ (d) and $\overline{\Delta_{a,i} \Delta_{b,j}}$ (e). The thin curves are obtained for $V/t = 0.1$ while the thick one for $V/t = 0.5$. Note that the correlations persist to distances of several order lattice spacing which corresponds on the SC-Islands size. We observe that the increasing of the hybridization tends to “suspend” and equalize the correlations $\overline{\Delta_{a,i} \Delta_{a,j}}$ and $\overline{\Delta_{b,i} \Delta_{b,j}}$. These results are normalized to be the unit for $|r_i - r_j| = 0$.

Appendix A: Mean Field Decoupling for interaction terms

where $\psi_{\uparrow,\downarrow} = a_{\uparrow,\downarrow}, b_{\uparrow,\downarrow}$. The ‘‘Fock condensates’’ are zero here, so $\langle \psi_{\uparrow}^{\dagger} \psi_{\downarrow} \rangle = \langle \psi_{\downarrow}^{\dagger} \psi_{\uparrow} \rangle = 0$ in Eqs. (A2, A3 and A4 below and consequently in Eq. (2).

$$\begin{aligned} \psi_{\uparrow}^{\dagger} \psi_{\downarrow}^{\dagger} \psi_{\downarrow} \psi_{\uparrow} = & \quad (A1) \\ & \langle \psi_{\downarrow} \psi_{\uparrow} \rangle \psi_{\uparrow}^{\dagger} \psi_{\downarrow}^{\dagger} + \langle \psi_{\uparrow}^{\dagger} \psi_{\downarrow}^{\dagger} \rangle \psi_{\downarrow} \psi_{\uparrow} - |\langle \psi_{\downarrow} \psi_{\uparrow} \rangle|^2 \\ & + \langle \psi_{\uparrow}^{\dagger} \psi_{\uparrow} \rangle \psi_{\downarrow}^{\dagger} \psi_{\downarrow} + \langle \psi_{\downarrow}^{\dagger} \psi_{\downarrow} \rangle \psi_{\uparrow}^{\dagger} \psi_{\uparrow} - \langle \psi_{\uparrow}^{\dagger} \psi_{\uparrow} \rangle \langle \psi_{\downarrow}^{\dagger} \psi_{\downarrow} \rangle \\ & - (\langle \psi_{\uparrow}^{\dagger} \psi_{\downarrow} \rangle \psi_{\downarrow}^{\dagger} \psi_{\uparrow} + \langle \psi_{\downarrow}^{\dagger} \psi_{\uparrow} \rangle \psi_{\uparrow}^{\dagger} \psi_{\downarrow}), \end{aligned}$$

$$\begin{aligned} -U_a \sum_i a_{i,\uparrow}^{\dagger} a_{i,\downarrow}^{\dagger} a_{i,\downarrow} a_{i,\uparrow} = & -U_a \sum_i [\langle a_{i,\downarrow} a_{i,\uparrow} \rangle a_{i,\uparrow}^{\dagger} a_{i,\downarrow}^{\dagger} + \langle a_{i,\uparrow}^{\dagger} a_{i,\downarrow}^{\dagger} \rangle a_{i,\downarrow} a_{i,\uparrow} - |\langle a_{i,\downarrow} a_{i,\uparrow} \rangle|^2 \\ & + \langle a_{i,\uparrow}^{\dagger} a_{i,\uparrow} \rangle a_{i,\downarrow}^{\dagger} a_{i,\downarrow} + \langle a_{i,\downarrow}^{\dagger} a_{i,\downarrow} \rangle a_{i,\uparrow}^{\dagger} a_{i,\uparrow} - \langle a_{i,\uparrow}^{\dagger} a_{i,\uparrow} \rangle \langle a_{i,\downarrow}^{\dagger} a_{i,\downarrow} \rangle], \end{aligned} \quad (A2)$$

$$\begin{aligned} -U_b \sum_i b_{i,\uparrow}^{\dagger} b_{i,\downarrow}^{\dagger} b_{i,\downarrow} b_{i,\uparrow} = & -U_b \sum_i [\langle b_{i,\downarrow} b_{i,\uparrow} \rangle b_{i,\uparrow}^{\dagger} b_{i,\downarrow}^{\dagger} + \langle b_{i,\uparrow}^{\dagger} b_{i,\downarrow}^{\dagger} \rangle b_{i,\downarrow} b_{i,\uparrow} - |\langle b_{i,\downarrow} b_{i,\uparrow} \rangle|^2 \\ & + \langle b_{i,\uparrow}^{\dagger} b_{i,\uparrow} \rangle b_{i,\downarrow}^{\dagger} b_{i,\downarrow} + \langle b_{i,\downarrow}^{\dagger} b_{i,\downarrow} \rangle b_{i,\uparrow}^{\dagger} b_{i,\uparrow} - \langle b_{i,\uparrow}^{\dagger} b_{i,\uparrow} \rangle \langle b_{i,\downarrow}^{\dagger} b_{i,\downarrow} \rangle]. \end{aligned} \quad (A3)$$

Defining $\Delta_{a,i} = -U_a \langle a_{i,\downarrow} a_{i,\uparrow} \rangle$, $\Delta_{b,i} = -U_b \langle b_{i,\downarrow} b_{i,\uparrow} \rangle$, $\langle n_{i,\sigma}^a \rangle = \langle a_{i,\sigma}^{\dagger} a_{i,\sigma} \rangle$ and $\langle n_{i,\sigma}^b \rangle = \langle b_{i,\sigma}^{\dagger} b_{i,\sigma} \rangle$, the interaction term reduces to

$$\begin{aligned} H_{int} = & \sum_i \Delta_{a,i} a_{i,\uparrow}^{\dagger} a_{i,\downarrow}^{\dagger} + \Delta_{a,i}^* a_{i,\downarrow} a_{i,\uparrow} + |\Delta_{a,i}|^2 / U_a - U_a [\langle n_{i,\uparrow}^a \rangle a_{i,\downarrow}^{\dagger} a_{i,\downarrow} + \langle n_{i,\downarrow}^a \rangle a_{i,\uparrow}^{\dagger} a_{i,\uparrow} - \langle n_{i,\uparrow}^a \rangle \langle n_{i,\downarrow}^a \rangle] \\ & + \sum_i \Delta_{b,i} b_{i,\uparrow}^{\dagger} b_{i,\downarrow}^{\dagger} + \Delta_{b,i}^* b_{i,\downarrow} b_{i,\uparrow} + |\Delta_{b,i}|^2 / U_b - U_b [\langle n_{i,\uparrow}^b \rangle a_{i,\downarrow}^{\dagger} b_{i,\downarrow} + \langle n_{i,\downarrow}^b \rangle b_{i,\uparrow}^{\dagger} b_{i,\uparrow} - \langle n_{i,\uparrow}^b \rangle \langle n_{i,\downarrow}^b \rangle]. \end{aligned} \quad (A4)$$

Appendix B: Hamiltonian in real space

Defining the base $\Psi^T = (a_{1\uparrow}^{\dagger}, \dots, a_{n^2\uparrow}^{\dagger}, b_{1\uparrow}^{\dagger}, \dots, b_{n^2\uparrow}^{\dagger}, a_{1\downarrow}, \dots, a_{n^2\downarrow}, b_{1\downarrow}, \dots, b_{n^2\downarrow})$, we can write HMF as $H_{MF} = \Psi^{\dagger} \mathcal{H} \Psi$, where $\mathcal{H} = \mathcal{H}_{4N \times 4N}$ for $N = n^2$. The Matrix \mathcal{H} is given by

$$\mathcal{H} = \begin{pmatrix} A & V & \Delta_{aa} & 0 \\ V & B & 0 & \Delta_{bb} \\ \Delta_{aa} & -A & 0 & -V \\ 0 & \Delta_{bb} & -V & -B \end{pmatrix}, \quad (B1)$$

where A , V , B , $\Delta_{\eta\eta}$ are matrices $N \times N$. Here, A is formed by on-site energy and hopping terms between electrons of the orbital a . The matrix B is formed by on-site energy and hopping terms between electrons of the orbital b . The matrix V is the subspace of the hybridization and $\Delta_{aa,bb}$ are formed by superconducting order parameters from orbitals a and b , respectively.

In order to diagonalize H_{MF} , we defined a matrix M . The matrix M acts in the basis Ψ as

$$\Psi = M \Phi \quad (B2)$$

or, explicitly

$$\begin{pmatrix} a_{\uparrow 1} \\ \vdots \\ a_{\uparrow N} \\ b_{\uparrow 1} \\ \vdots \\ b_{\uparrow N} \\ a_{\downarrow 1} \\ \vdots \\ a_{\downarrow N} \\ b_{\downarrow 1} \\ \vdots \\ b_{\downarrow N} \end{pmatrix} = \begin{pmatrix} M_{1,1} & \cdots & M_{1,N} & M_{1,N+1} & \cdots & M_{1,2N} & M_{1,2N+1} & \cdots & M_{1,3N} & M_{1,3N+1} & \cdots & M_{1,4N} \\ \vdots & \vdots & \vdots & \ddots & \vdots & \vdots & \vdots & \vdots & \vdots & \vdots & \vdots & \vdots \\ M_{N,1} & \cdots & M_{N,N} & M_{N,N+1} & \cdots & M_{N,2N} & M_{N,2N+1} & \cdots & M_{N,3N} & M_{N,3N+1} & \cdots & M_{N,4N} \\ M_{N+1,1} & \cdots & M_{N+1,N} & M_{N+1,N+1} & \cdots & M_{N+1,2N} & M_{N+1,2N+1} & \cdots & M_{N+1,3N} & M_{N+1,3N+1} & \cdots & M_{N+1,4N} \\ \vdots & \vdots & \vdots & \ddots & \vdots & \vdots & \vdots & \vdots & \vdots & \vdots & \vdots & \vdots \\ M_{2N,1} & \cdots & M_{2N,N} & M_{2N,N+1} & \cdots & M_{2N,2N} & M_{2N,2N+1} & \cdots & M_{2N,3N} & M_{2N,3N+1} & \cdots & M_{2N,4N} \\ M_{2N+1,1} & \cdots & M_{2N+1,N} & M_{2N+1,N+1} & \cdots & M_{2N+1,2N} & M_{2N+1,2N+1} & \cdots & M_{2N+1,3N} & M_{2N+1,3N+1} & \cdots & M_{2N+1,4N} \\ \vdots & \vdots & \vdots & \ddots & \vdots & \vdots & \vdots & \vdots & \vdots & \vdots & \vdots & \vdots \\ M_{3N,1} & \cdots & M_{3N,N} & M_{3N,N+1} & \cdots & M_{3N,2N} & M_{3N,2N+1} & \cdots & M_{3N,3N} & M_{3N,3N+1} & \cdots & M_{3N,4N} \\ M_{3N+1,1} & \cdots & M_{3N+1,N} & M_{3N+1,N+1} & \cdots & M_{3N+1,2N} & M_{3N+1,2N+1} & \cdots & M_{3N+1,3N} & M_{3N+1,3N+1} & \cdots & M_{3N+1,4N} \\ \vdots & \vdots & \vdots & \ddots & \vdots & \vdots & \vdots & \vdots & \vdots & \vdots & \vdots & \vdots \\ M_{4N,1} & \cdots & M_{4N,N} & M_{4N,N+1} & \cdots & M_{4N,2N} & M_{4N,2N+1} & \cdots & M_{4N,3N} & M_{4N,3N+1} & \cdots & M_{4N,4N} \end{pmatrix} \begin{pmatrix} \alpha_{\uparrow 1} \\ \vdots \\ \alpha_{\uparrow N} \\ \alpha_{\uparrow 1} \\ \vdots \\ \alpha_{\uparrow N} \\ \alpha_{\downarrow 1} \\ \vdots \\ \alpha_{\downarrow N} \\ \alpha_{\downarrow 1} \\ \vdots \\ \alpha_{\downarrow N} \end{pmatrix} \quad (\text{B3})$$

such that, the new base $\Phi^T = (\alpha_{1\uparrow}^\dagger, \dots, \alpha_{N\uparrow}^\dagger, \alpha_{1\uparrow}^\dagger, \dots, \alpha_{N\uparrow}^\dagger, \alpha_{1\downarrow}, \dots, \alpha_{N\downarrow}, \alpha_{1\downarrow}, \dots, \alpha_{N\downarrow})$ is a base where H_{MF} become diagonal

$$M^\dagger H_{MF} M = \text{diag}(-E_1 \dots - E_{2N}; E_{2N} \dots E_1) \quad (\text{B4})$$

We call attention to fact that the columns of M are the eigenvectors of H_{MF} . We organized the eigenvalues of H_{MF} from the lesser to greater values (i. e. $-E_1 \dots - E_{2N}, E_{2N} \dots E_1$) and therefore, note that, the last $2N$ columns of M contain all eigenvectors that are related to positive energies of the Hamiltonian H_{MF} .

The Bogoliubov-Valatin transformations can be defined according the Eq. B3 in the following way

$$a_{i,\uparrow} = \sum_{n'=1}^N [M_{i,2N+n'} \alpha_{2N+n',\uparrow} - M_{i,3N+n'} \alpha_{3N+n',\downarrow}^\dagger], \quad (\text{B5})$$

$$b_{i,\uparrow} = \sum_{n'=1}^N [M_{i+N,2N+n'} \alpha_{2N+n',\uparrow} - M_{i+N,3N+n'} \alpha_{3N+n',\downarrow}^\dagger], \quad (\text{B6})$$

$$a_{i,\downarrow} = \sum_{n'=1}^N [M_{i+2N,2N+n'} \alpha_{2N+n',\uparrow} + M_{i+2N,3N+n'}^* \alpha_{3N+n',\downarrow}^\dagger], \quad (\text{B7})$$

$$b_{i,\downarrow} = \sum_{n'=1}^{N^2} [M_{i+3N,2N+n'} \alpha_{2N+n',\uparrow} + M_{i+3N,3N+n'}^* \alpha_{3N+n',\downarrow}^\dagger], \quad (\text{B8})$$

where the sum only runs over n' corresponding to positive eigenvalues. The Eqs. B5-B8 are nothing more than the product of a line of M by the vector Φ .

-
- [1] J. G. Bednorz and K. A. Müller, Z. Phys. B: Condens. Matter **64**, 189 (1986); K. A. Müller and J. G. Bednorz, Science **237**, 1133 (1987).
- [2] Y. Maeno, H. Hashimoto, K. Yoshida, S. Nishizaki, T. Fujita, J. G. Bednorz, and F. Lichtenberg, Nature London **372**, 532 (1994).
- [3] J. Nagamatsu, N. Nakagawa, T. Muranaka, Y. Zenitani, and J. Akimitsu, Nature London **410**, 63 (2001).
- [4] Y. Kamihara, H. Hiramatsu, M. Hirano, R. Kawamura, H. Yanagi, T. Kamiya, and H. Hosono, J. Am. Chem. Soc. **128**, 10012 (2006).
- [5] Y. Kamihara, T. Watanabe, M. Hirano, and H. Hosono, J. Am. Chem. Soc. **130**, 3296 (2008).
- [6] J. Nagamatsu, N. Nakagawa, T. Muranaka, Y. Zenitani, and J. Akimitsu, Nature London **410**, 41 (2001).
- [7] Y. Wang, T. Plackowski, A. Junod, Physica C **355**, 179 (2001).
- [8] F. Bouquet, R. A. Fisher, N. E. Phillips, D. G. Hinks, and J. D. Jorgensen, Phys. Rev. Lett. **87**, 047001 (2001).
- [9] H. D. Yang, J.-Y. Lin, H. H. Li, F. H. Hsu, C. J. Liu,

- S.-C. Li, R.-C. Yu, and C.-Q. Jin, Phys. Rev. Lett. **87**, 167003 (2001).
- [10] P. Szabó, P. Samuely, J. Kačmarčík, T. Klein, J. Marcus, D. Fruchart, S. Miraglia, C. Marcenat, and A. G. M. Jansen, Phys. Rev. Lett. **87**, 137005 (2001).
- [11] F. Giubileo, D. Roditchev, W. Sacks, R. Lamy, D. X. Thanh, J. Klein, S. Miraglia, D. Fruchart, J. Marcus, and Ph. Monod, Phys. Rev. Lett. **87**, 177008 (2001).
- [12] X. K. Chen, M. J. Konstantinović, J. C. Irwin, D. D. Lawrie, and J. P. Franck, Phys. Rev. Lett. **87**, 157002 (2001).
- [13] S. Tsuda, T. Yokoya, T. Kiss, Y. Takano, K. Togano, H. Kito, H. Ihara, and S. Shin, Phys. Rev. Lett. **87**, 177006 (2001).
- [14] J. Geerk, R. Schneider, G. Linker, A. G. Zaitsev, R. Heid, K.-P. Bohnen, and H. v. Löhneysen, Phys. Rev. Lett. **94**, 227005 (2005).
- [15] A. Y. Liu, I. I. Mazin, and J. Kortus, Phys. Rev. Lett. **87**, 087005 (2001).
- [16] A. Moreo, M. Daghofer, J. A. Riera, and E. Dagotto, Phys. Rev. B **79**, 134502 (2009).
- [17] H. J. Choi, D. Roundy, H. Sun, M. L. Cohen, and S. G. Louie, Nature London **418**, 758 (2002).
- [18] C. E. Matt, D. Sutter, A. M. Cook, Y. Sassa, M. Manson, O. Tjernberg, L. Das, M. Horio, D. Destraz, C. G. Fatuzzo, et al., Nature Commun. **9**, 972 (2018).
- [19] M. V. Feigel'man, L. B. Ioffe, V. E. Kravtsov, and E. A. Yuzbashyan, Phys. Rev. Lett. **98**, 027001 (2007).
- [20] B. Sacépé, T. Dubouchet, C. Chapelier, et al., Nature Phys. **7**, 239 (2011).
- [21] B. Sacépé, M. Feigel'man and T. M. Klapwijk, Nature Phys. **16**, 734 (2020).
- [22] A. M. Goldman and N. Marković, Phys. Today **51** (11), 39 (1998).
- [23] P. W. Anderson, J. Phys. Chem. Solids **11**, 26 (1959).
- [24] A. A. Abrikosov and L. P. Gorkov, Zh. Éksp. Teor. Fiz. **36**, 319 (1959) [Sov. Phys. JETP **9**, 220 (1959)].
- [25] D. Belitz and T. Kirkpatrick, Rev. Mod. Phys. **66**, 261 (1994).
- [26] A. Ghosal, M. Randeria, and N. Trivedi, Phys. Rev. B **65**, 014501 (2001).
- [27] S. M. Ramos et al., Phys. Rev. Lett. **105**, 126401 (2010).
- [28] H. Sakakibara, K. Suzuki, H. Usui, K. Kuroki, R. Arita, D. Scalapino and H. Aoki, Phys. Rev. B **86**, 134520 (2012).
- [29] L. Deng, Y. Zheng, Z. Wu, S. Huyan, H. Wu, Y. Nie, K. Cho and C. Chu, Proc. Natl. Acad. Sci. USA **116**, 2004 (2019).
- [30] H. Caldas, F. S. Batista, M. A. Continentino, F. Deus, and D. Nozadze, Ann. Phys. **384**, 211 (2017).
- [31] A. Y. Kitaev, Sov. Phys. Usp. **44**, 131 (2001).
- [32] R. Wakatsuki, M. Ezawa, Y. Tanaka, and N. Nagaosa, Phys. Rev. B **90**, 014505 (2014).
- [33] M. A. Continentino, H. Caldas, D. Nozadze, and N. Trivedi, Phys. Lett. A **378**, 3340 (2014).
- [34] M. A. R. Griffith, E. Mamani, L. Nunes, and H. Caldas, Phys. Rev. B **101**, 184514 (2020).
- [35] M. Foglio, L. Falicov, Phys. Rev. B **20**, 4554 (1979).
- [36] A. A. Aligia, E. Gagliano, L. Arrachea, and K. Hallberg, Eur. Phys. J. B **5**, 371 (1998).
- [37] N. N. Bogoljubov II Nuovo Cimento (1955-1965) volume **7**, 794 (1958); J. G. Valatin II Nuovo Cimento (1955-1965) volume **7**, 843 (1958).
- [38] J.-PetriMartikainen, J. Larson, Phys. Rev. A **86**, 023611 (2012).
- [39] S. Yin, J. E. Baarsma, M. O. J. Heikkinen, J.-P. Martikainen, P. Torma, Phys. Rev. A **86**, 053616 (2015).
- [40] H. Caldas, A. Celes, D. Nozadze, Ann. Phys. **394**, 17 (2018).
- [41] V. F. Gantmakher, V. T. Dolgoplov, Phys.-Usp. **53**, 1 (2010).
- [42] We thank N. Trivedi for pointing out this fact.
- [43] Y. Dubi, Y. Meir, Y. and Y. Avishai, Nature **449**, 876-880 (2007).
- [44] D. B. Haviland, Y. Liu, and A. M. Goldman, Phys. Rev. Lett. **62**, 2180 (1989); J. M. Valles, R. C. Dynes, and J. P. Garno, ibid. **69**, 3567 (1992).
- [45] A. E. White, R. C. Dynes, and J. P. Garno, Phys. Rev. B **33**, 3549 (1986).
- [46] H. M. Jaeger, D. B. Haviland, A. M. Goldman, and B. G. Orr, Phys. Rev. B **34**, 4920 (1986).
- [47] D. Shahar and Z. Ovadyahu, Phys. Rev. B **46**, 10917 (1992).
- [48] J. Kim, V. Chua, G. Fiete et al., Nature Phys. **8**, 464 (2012).
- [49] H. Caldas, R. O. Ramos, Phys. Rev. B **80** (11), 115428 (2009).